ARTICLE

Probing the catalytic potential of oxygen and sulfur chalcogen bond interactions

Binzhou Lin, Hao Liu, Harrison M. Scott, Ishwor Karki, Erik C. Vik, Perry J. Pellechia and Ken D. Shimizu*

Received 00th January 20xx,
Accepted 00th January 20xx

DOI: 10.1039/x0xx00000x

Non-covalent chalcogen bond (ChB) interactions have found utility in many fields, including organocatalysis. To assess the potential of ChB interactions of the most abundant chalcogens (oxygen and sulfur) in catalysis, the kinetic effect of S and O ChBs were experimentally measured using a series of molecular rotors. The rotors were designed to form stabilizing ChB interactions in their bond rotations in transition states. The lower rotational barriers and increased rates of rotation were monitored by 2D EXSY ^{1}HNMR. Despite the lack of the strong electron-withdrawing groups, a properly oriented sulfur lowered the rotational barriers of by as much as -7.2 kcal/mol. Oxygen rotors also could form ChB interactions but required electron withdrawing groups. These findings suggest that ChB interactions can be used to design efficient catalysts for a variety of reactions. The geometric propensities of the interactions showed that the oxygen and sulfur interactions had different orbital-orbital components the corresponded to their polarizabilities. The strong correlation between the strength of the interactions and ESP provides a valuable tool for the rational design of future ChB catalysts.

Introduction

The chalcogen bond (ChB) is an attractive interaction between an electron-poor region on a chalcogen atom (O, S, Se, Te) with an electron-rich region of a second group.[1–3] ChBs are relatively new non-covalent interactions. Yet, they have already found applications in molecular recognition,[4–7] drug design,[8–10] crystal engineering,[2,11,12] and organic semiconductors.[13] A particularly promising application has been in organocatalysis.[14–17] For example, Matile has developed a organocatalyst which activates pyridines, quinolines, and imines for reduction using selenium chalcogen bonds (Figure 1a).[14,18] Elsewhere, Smith proposed that intramolecular sulfur chalcogen bonding interactions were essential in an isothiourea-catalyzed asymmetric annulation reaction (Figure 1b).[19] Additional examples of chalcogen bonding promoted or catalyzed reactions include: enantioselective acylation of alcohols,[20–22] hydrogenation,[14] bromination,[23] halide abstraction,[24] Michael addition,[25] Rauhut-Currier-type reactions,[17] ketone cyanosilylation,[26] and Diels-Alder reactions.[27]

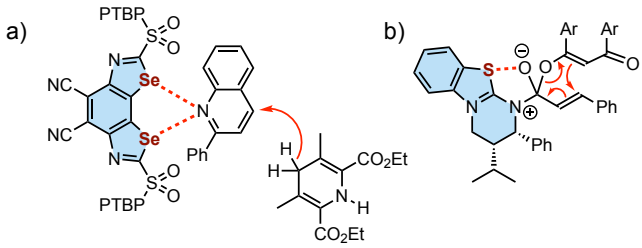

Fig. 1 Examples of chalcogen bonding (ChB) interactions in organocatalysis, highlighting the role of the ChB interaction (dotted line) in the key transition state or intermediate complexes.[18,19]

While there have been experimental and theoretical studies of chalcogen bonding interactions,[2,11,12,28–31] few have directly examined their abilities to effect reaction rates[32] and kinetics[33] via the stabilization of transition states and intermediates. Most studies have focused on the ChB interactions of thermodynamically stable structures such as those in host-guest complexes or self-assembly.[5,34,35] The stability trends for non-covalent interactions formed in transition states may differ due to their hypervalent atoms and distorted bond lengths and angles. Therefore, the goal of this study was to quantitatively assess the catalytic abilities of the ChB interaction and compare them to other common non-covalent interactions used in organocatalysts such as hydrogen bonding and n → π* interactions. We were particularly interested in the smallest chalcogens, oxygen and sulfur, which are the most abundant and commonly found in organic frameworks.

Measuring the kinetic effects of non-covalent interactions is challenging as transition states are unstable structures that are difficult to probe. In addition, transition state

[a] *Department of Chemistry and Biochemistry, University of South Carolina, Columbia, SC 29208, USA.*

† Footnotes relating to the title and/or authors should appear here.
Electronic Supplementary Information (ESI) available: [details of any supplementary information available should be included here]. See DOI: 10.1039/x0xx00000x

structures and mechanisms can change over the course of a study. Thus, we developed a simple kinetic model system based on an *N*-phenylsuccinimide molecular rotor (Figure 2).[36–39] Rotation of the central N_{imide}-C_{phenyl} single bond is a unimolecular kinetic process with a single barrier and a well-defined planar transition state where interacting groups are forced close together. Rotors which can form stabilizing intramolecular ChBs in the TS will have lower rotational barriers and spin faster. The TS stabilizing effects of the ChB (E_{int}) can be quantified by comparing the barrier to control rotors that cannot form stabilizing TS interactions (E_{steric}).

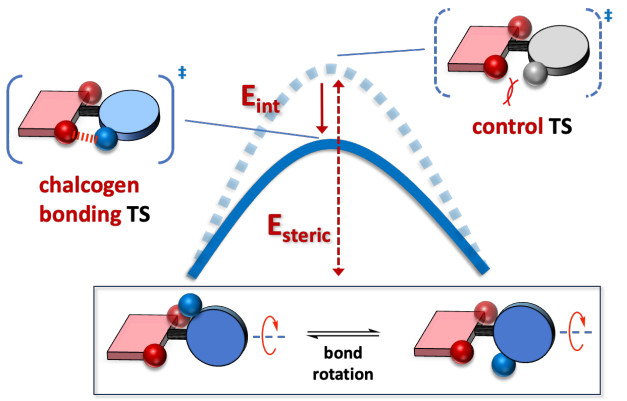

Fig. 2 Schematic representation of the energy profile of the bond rotation process that highlights the strategy of isolating the stabilizing chalcogen bonding (ChB) interactions (E_{int}) in the TS by comparison with a steric control rotor which measures the steric component of the rotational barrier (E_{steric}).

We have successfully employed *N*-phenylsuccinimide rotors to measure and study the kinetic effects other non-covalent interactions such as hydrogen bonding and *n* → π* interactions.[36–39] This provides support for the effectiveness of the molecular rotors approach and also provides the opportunity to compare the kinetic effects of the ChB interactions with other non-covalent interactions that have been used in organocatalysts.

The larger chalcogens (Se, Te) are known to form stronger ChB interactions as they are more polarizable which enables the formation of a larger *σ*-hole. Our main question was whether the smaller chalcogens (S, O) also had potential in organocatalysis by measuring their abilities to affect kinetic processes. While the weaker ChB interactions of sulfur and oxygen would mitigate their utility, this is offset by their greater abundance and ease of incorporation into organic frameworks.

Therefore, our objectives were to employ the molecular rotors to: 1) measure the TS stabilizing abilities sulfur and oxygen ChB interactions, 2) examine the influence of interaction geometry and electron withdrawing groups 3) compare the kinetic effects of ChB interactions with other non-covalent interactions and 4) to develop predictive models to guide researches in designing new ChB organocatalysts.

N-phenylsuccinimide sulfur rotors **1** and oxygen rotors **2** were designed to measure the TS stabilizing effects of the sulfur ChB and oxygen ChB interactions (Figure 3). Due to the steric interactions of the imide C=O groups, the rotors display restricted rotation leading the formation of *syn*- and *anti*-conformers (Figure 3). The imide C=O groups can also form TS stabilizing chalcogen bonding interactions with the sulfur or oxygen atoms in the 2-position of the *N*-phenyl unit of rotors **1** and **2**.

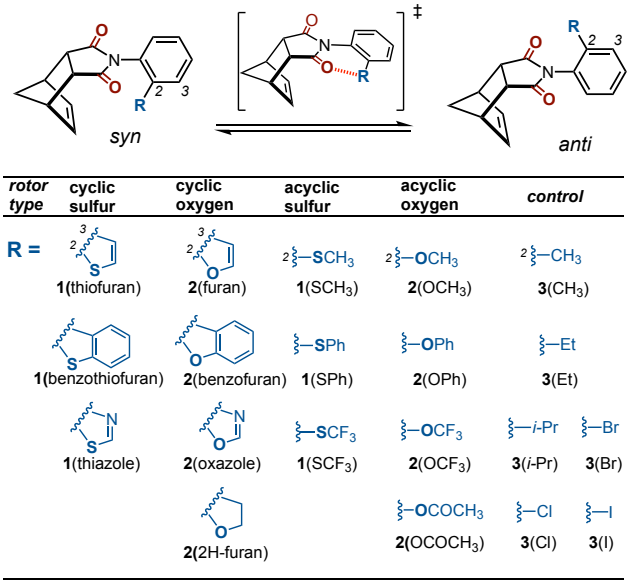

Fig. 3. Conformational *syn-anti* equilibrium of the *N*-phenylsuccinimide molecular rotors **1** arising from bond rotation around the C-N bond. The R-groups are attached at the 2-position of the *N*-phenyl unit with the all the cyclic structures which were fused at the *ortho*- and *meta*-positions.

There are two general classes of ChB rotors: cyclic and acyclic. The cyclic rotors have a chalcogen heterocycle fused to the 2- and 3-positions of the *N*-phenyl unit. The cyclic constraint fixes the geometry of chalcogen atom at the 2-position into a favorable geometry for the ChB interaction (vide infra). The acyclic rotors allow greater conformational freedom of the chalcogen group, and in most cases, the rotors adopt a poor ChB geometry, with the chalcogen *σ*-hole is perpendicular to the imide oxygen lone pair. In addition to exploring the importance of chalcogen atom size and geometry, variations in conjugation and electron withdrawing abilities of the groups attached to the sulfur and oxygen atoms assessed the role of electrostatics and *σ*-hole size.

To assist in separating the stabilizing ChB and destabilizing steric components of the rotational barriers, control rotors **3** were designed that lack chalcogen atoms and cannot form ChB interactions. Therefore, the rotational barriers of rotors **3** provided a direct measure of the steric component. We have previously successfully utilized this set of control rotors to isolate the TS stabilizing of n → π*,[38] n → π(aromatic)[37], and pnictogen interactions.[40]

Results and Discussion

Experimental measurements

The new ChB rotors **1** and **2** were synthesized by thermal condensation of the appropriate *ortho*-substituted aniline with *cis*-5-norbornene-*endo*-2,3-dicarboxylic anhydride to form the *N*-phenylsuccinimide rotors (Figure 4, see ESI section 2).[38,40,41] The imide cyclization reaction is high yielding, does not require additional reagents or catalysts, and functional group tolerant, enabling the rapid assembly of rotors with a variety of chalcogen groups. The structures of several of the rotors (**1**(benzothiofuran), **1**(thiazole), **1**(SPh), **2**(benzofuran)) were also confirmed by X-ray crystallography (ESI). As expected, the steric interactions between the imide carbonyl and the R-groups in the 2-position lead to distinct *syn*- or *anti*-conformers.

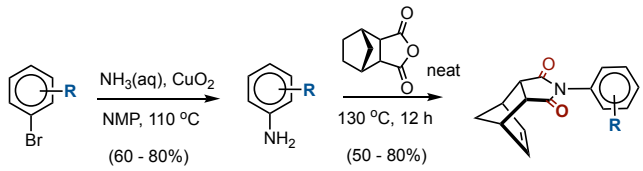

Fig. 4 General scheme for the two-step synthesis of the chalcogen rotors.

The rotational barriers ($\Delta G^{\ddagger}_{exp}$) were measured using 2D EXSY NMR in TCE-d2. All rotors displayed restricted rotation, as separate peaks were observed in the NMR spectra for the *syn*- and *anti*-conformers below their coalescence temperatures (-50 to >140 °C). The rates of exchange between the *syn*- and *anti*-conformers was measured over a range of temperatures using 2D EXSY of the ^{1}H NMR spectra of the norborene alkene protons.[38,40] The resulting $\Delta H^{\ddagger}_{exp}$ and $\Delta S^{\ddagger}_{exp}$ values from the Eyring plots were used to calculate $\Delta G^{\ddagger}_{exp}$ at a common temperature (298.15 K) to allow direct comparisons. The error in $\Delta G^{\ddagger}_{exp}$ was estimated as ± 0.2 kcal/mol based on previous literature precedence.[42,43]

The NMR measured rotational barriers ($\Delta G^{\ddagger}_{exp}$) of the chalcogen rotors varied from 12.0 to 24.2 kcal/mol (Table 1). In general, the sulfur rotors **1** had higher barriers than the oxygen rotors **1**, which is consistent with the larger size of the sulfur atoms, leading to greater steric interactions in the TS. The cyclic rotors had lower barriers than the acyclic rotors due to the constraints provided by the fused 5-membered rings moving the chalcogen atom away from the opposing C=O oxygen.

Table 1 Measured parameters ($\Delta G^{\ddagger}_{exp}$, E_{steric}, E_{int}) for molecular rotors **1**, **2**, and **3** and the steric parameter *B*-value for the R-groups in the 2-position of the *N*-phenylsuccinimide rotors. The values for all parameters are in units of kcal/mol.

rotors	type	$\Delta G^{\ddagger}_{exp}$[a]	*B*-value[b]	E_{steric}[c]	E_{int}[d]
1(thiofuran)	cyclic	14.9	*5.2*	19.7	-4.8
1(benzothiofuran)	cyclic	14.9	*5.5*	19.9	-5.0
1(thiazole)	cyclic	12.0	*4.6*	19.2	-7.2
2(furan)	cyclic	15.0	*1.9*	17.0	-2.0
2(benzofuran)	cyclic	14.9	*2.0*	17.1	-2.2
2(oxazole)	cyclic	12.0	*1.5*	16.7	-4.7
2(2H-furan)	cyclic	15.8	*1.6*	16.8	-1.0
1(SCH_3)	acyclic	22.5	8.6	22.4	+0.1
1(SPh)	acyclic	21.8	8.3	22.2	-0.4
1(SCF_3)	acyclic	21.8	*8.2*	22.1	-0.3
2(OCH_3)	acyclic	20.2	5.6	20.0	+0.2[f]
2(OPh)	acyclic	18.2	*4.2*	18.9	-0.7[f]
2(OCF_3)	acyclic	17.9	5.5	19.9	-2.0
2($OCOCH_3$)	acyclic	16.3	*5.4*	19.8	-3.5
3(CH_3)	acyclic	21.7[e]	7.4	21.4	f
3(Et)	acyclic	22.0[e]	8.7	22.5	f
3(*i*-Pr)	acyclic	23.6[e]	11.1	24.4	f
3(Cl)	acyclic	22.1[e]	7.7	21.7	f
3(Br)	acyclic	23.1[e]	8.7	22.5	f
3(I)	acyclic	23.7[e]	10.0	23.5	f
3(CF_3)	acyclic	24.2[e]	10.5	23.9	f

[a]measured by EXSY ^{1}H NMR. [b]values from literature or calculated (*italics*) at the B3LYP / 6-31G*.[44] [c]calculated from equation 2. [d]calculated from equation 1. [e]values previously reported.[38,40] [f]rotor was used to calculate the steric trendline.

Confirmation that the rotors formed stabilizing chalcogen interactions were provided by analysis of the experimental and computational rotational barriers. The first indications of the ChB interactions were provided by comparison of $\Delta G^{\ddagger}_{exp}$ values for structurally similar pairs of sulfur and oxygen rotors. The barriers for the sulfur rotors were expected to be higher, due to the larger size and steric interactions of the sulfur versus oxygen atoms. However, the more polarizable sulfur atom is known to form stronger ChB interactions than the less polarizable oxygen atom. [30] Therefore, if the sulfur rotors had similar or lower barriers than the oxygen rotors, this could be an indication of the presence of additional TS stabilizing ChB interactions in the sulfur rotors. This was what was observed when comparing similar cyclic sulfur and oxygen rotors. For example, the sulfur rotor **1**(thiofuran) and the oxygen rotor **2**(furan) had very similar $\Delta G^{\ddagger}_{exp}$ values (14.9 and 15.0 kcal/mol). The two other pairs of structurally similar cyclic chalcogen rotors also had similar barriers that went against the steric trends. The rotors **1**(benzothiofuran) and **2**(benzofuran) had the same barriers (14.9 and 14.9 kcal/mol). Likewise, the rotor pair **1**(thiazole) and **2**(oxazole) had the same barriers (12.0 and 12.0 kcal/mol).

In contrast, the $\Delta G^{\ddagger}_{exp}$ values for the acyclic chalcogen rotors followed the expected steric trends and did not show evidence of stabilizing ChB interactions. For example, rotor **1**(SCH_3) had a higher barrier versus the oxygen rotor **2**(OCH_3) (22.5 vs 20.2 kcal/mol). The other acyclic sulfur and oxygen pairs (**1**(SPh) and **2**(OPh), **1**(SCF_3) and **2**(OCF_3)) also followed

the steric trends with the sulfur rotors having a higher barrier than the oxygen rotors. These initial comparisons suggest that the cyclic chalcogen rotors form TS stabilizing ChB interactions. Whereas, the acyclic chalcogen rotors do not. These conclusions were corroborated by the computational analyses below.

Computational analyses

Computational studies provided further support for the formation of TS stabilizing ChB interactions in the cyclic sulfur rotors and an explanation for the absence of ChB interactions in the acyclic sulfur rotors. The ground state and transition state structures were calculated at the B3LYP-D3/6-311G* level of theory. The ground state structures were consistent with the x-ray structures. Support for the accuracy of the transition state structures was provided by the ability to reproduce the measured barriers (Table 2) with a good level of accuracy (±1.1 kcal/mol). The accuracy was similar for rotors which formed and did not form ChB interactions (see ESI). The level of accuracy and ability to model TS interactions were consistent with our previous computational studies of *N*-phenylsuccinimide rotors.[38,40]

Analyses of the cyclic sulfur rotor TS structures were consistent with the formation of stabilizing chalcogen interactions (Figure 5). The distances between the C=O oxygen and the sulfur atoms (Table 2) were significantly shorter than the sum of the VDW radii for S and O, which is 3.32 Å. For example, the distances (2.535 to 2.580 Å) for **1**(thiofuran), **1**(benzothiofuran), and **1**(thiazole) fall within the range for ChB bonds observed in crystallographic and theory studies (2.4-3.0 Å).[8,32,45] These distances were also similar to the intramolecular chalcogen bonds in the organocatalysts such as the *N*-acyl isothiourea systems highlighted in Figure 1b.[32]

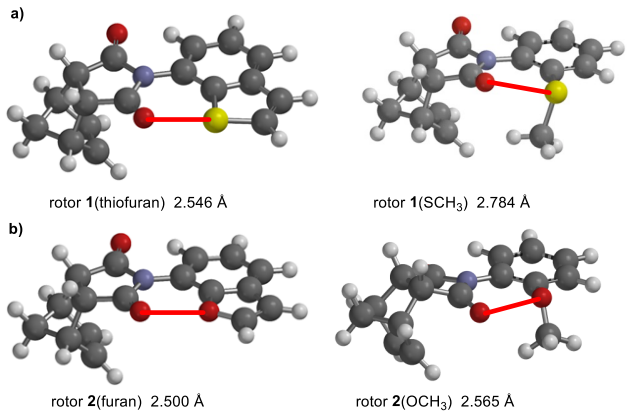

Fig. 5 a) Comparison of the C=O•••chalcogen TS distances of cyclic rotor **1**(thiofuran) and acyclic rotor **1**(SCH_3). b) Comparison of the C=O•••chalcogen TS distances of cyclic rotor **2**(furan) and acyclic rotor **2**(OCH_3).

Comparison of the TS conformations of the cyclic and acyclic sulfur rotors **1** confirmed the importance of the interaction geometry in forming a strong ChB interaction (Figure 5). Theoretical studies have shown that a strong ChB interaction adopt a geometry where the σ-hole of the chalcogen is aligned with the lone pair of the ChB acceptor.[3,46,47] The TS structures of the cyclic chalcogen rotors are constrained in a favorable ChB geometry with near linear O•••S-C angles from 175° to 178°. This is consistent with the cyclic **1** rotors forming stabilizing ChB interactions.

Table 2 Measurements from the calculated TS structures (B3LYP-D3/6-311G*)

rotors	angle[a] O•••Ch-C (deg)	distance[a] O•••Ch (Å)	NBO[b] (kcal/mol)	ESP[c] (kcal/mol)
1(thiofuran)	177.7	2.546	-6.5	12.5
1(benzothiofuran)	177.8	2.535	-6.9	15.0
1(thiazole)	175.1	2.580	-5.8	22.0
2(furan)	152.3	2.503	-0.5	-12.5
2(benzofuran)	151.4	2.500	-0.5	-10.0
2(oxazole)	157.7	2.512	-0.6	7.5
2(2H-furan)	146.6	2.510	0.0	-15.0
1(SCH_3)	76.0[d] (160.0)[e]	2.591[d] (2.784)[e]	0.0[d] (-3.7)[e]	-22.0[d] (3.0)[e]
1(SPh)	77.1	2.814	0.0	-17.5
1(SCF_3)	87.7	2.783	0.0	-14.0
2(OCH_3)	74.0	2.565	0.0	-22.5
2(OPh)	75.0	2.527	0.0	-17.5
2(OCF_3)	89.7	2.524	0.0	-5.0
2($OCOCH_3$)	74.7	2.579	0.0	0.5

[a]Ch = oxygen or sulfur. [b]second order NBO perturbation energies calculated at the ωB97M-V/6-311+G* level of theory for the sum of orbital interactions between the C=O oxygen lone pairs and the chalcogen atom. [c]calculated at the ωB97M-V/6-311+G*level of theory at the position on the chalcogen atom closest to the C=O oxygen in the TS. [d]perpendicular TS of **1**(SCH_3). [e]planar TS of **1**(SCH_3).

In contrast, the acyclic sulfur rotors had difficulty adopting a favorable ChB interaction geometry (Figure 5). The TS structures of **1**(SCH_3), **1**(CF_3) and **1**(SPh) had the thioether group twisted out of the plane of the *N*-phenyl group. This perpendicular geometry avoids the destabilizing steric interactions between the R-group of the thioether and adjacent C-H groups of the phenyl ring (Figure 6). However in doing so, the sulfur σ-hole is out of alignment with the oxygen lone pair as the O•••S-C bond angles were far from linear (76.0° to 87.7°) as shown in Table 2. The absence of strong ChB interactions in the acyclic sulfur rotors was evident from the consistently longer C=O•••S distances (2.78 to 2.81 Å) in comparison to the cyclic rotors (2.54 to 2.58 Å). The shorter distances for the cyclic sulfur rotors are even more impressive given the framework constraints that favor the opposite trends. The fused five-membered rings of the cyclic rotors pull the sulfur away from the opposing C=O group in the TS due to the smaller C_3-C_2-S bond angle favoring longer S•••O distances (Figure 6). By comparison, the acyclic rotor has larger C_3-C_2-S bond angles favoring shorter ChB distances.

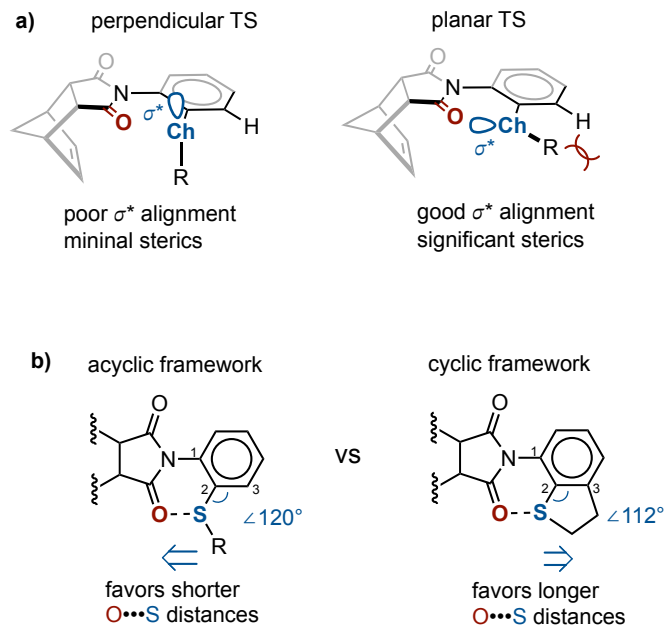

Fig. 6 Comparison of the geometric variations in the TS structures of the acyclic chalcogen rotors.

The one outlier in the trends for the acyclic sulfur rotors was **1**(SCH_3) which has perpendicular and planar TS structures that are very close in energy. A comparison of the two TS geometries provided further proof for the importance of proper alignment of the σ-hole in the sulfur ChB interaction. The planar TS has good alignment of the sulfur σ-hole with the C=O oxygen with a ChB bond angle of 160°. The presence of a stabilizing ChB interaction was evident from the short S•••O distance of 2.59 Å. In contrast, the perpendicular TS had poor alignment with a bond angle of 76° and a much longer S•••O distance of 2.78 Å, indicative of a weaker ChB interaction. While **1**(SCH_3) has the ability to form a ChB interaction in the planar TS, the TS stabilizing effects of the interaction are offset by the additional steric interactions that are formed by the CH_3 and thus, the similarity in the energies of the perpendicular and planar geometries. For the other acyclic rotors **1**(Ph) and **1**(CF_3), the destabilizing steric interactions in the planar geometry are larger and thus the perpendicular geometry is favored.

Quantitative empirical measurement of the ChB interactions

To better understand the trends and to evaluate its potential in effecting reaction rates, we quantitatively measured the magnitude of the TS stabilization by the ChB interactions. Our approach relies on decomposing the rotational barrier ($\Delta G^{\ddagger}_{exp}$) into a destabilizing steric (E_{steric}) and a stabilizing non-covalent component (E_{int}). Thus, E_{int} can be isolated by subtracting E_{steric} from $\Delta G^{\ddagger}_{exp}$ (equation 1). Therefore, the key to measuring E_{int} is to find appropriate steric control rotors to measure E_{steric}. In the above studies, pairwise comparisons were used where the ChB forming rotors were compared with structurally similar rotors that either do not form or form weaker ChB interactions. The difficulty with this analysis is that there are not always structurally similar control rotors available for comparison.

$$E_{int} = \Delta G^{\ddagger}_{exp} - E_{steric} \quad \text{(equation 1)}$$

$$E_{steric} = 0.8061(B\text{-value}) + 15.47 \quad \text{(equation 2)}$$

$$E_{int} = \Delta G^{\ddagger}_{exp} - 0.8061(B\text{-value}) - 15.47 \quad \text{(equation 3)}$$

Therefore, a systematic approach was employed to generate an ideal steric control for each chalcogen rotor. The barriers from a previously measured series of control rotors **3** were used to generate equation 2 for E_{steric} for any size R-group.[38,40] Rotors **3** have R-groups that lack a chalcogen atom and cannot form ChB or other stabilizing non-covalent interactions with the C=O group. Thus, we assumed that their barriers were due only to the steric component, E_{steric}. The size of the R-groups in rotors were quantitatively assessed using Mazzanti's steric parameter, *B*-value (Table 1), which was chosen because the parameter is based on the rotational barrier of a similar biaryl molecular rotor.[44] Confirmation of the ability of *B*-value to assess the steric size of the R-groups in the *N*-phenylsuccinimide rotors as provided by the good linear correlation of the $\Delta G^{\ddagger}_{exp}$ values of rotors **3** with *B*-value gave a linear correlation (Figure 7, black filled squares) with *B*-value demonstrating that the rotational barriers of the control rotors 3 were primarily due to the steric size of their R-groups.

A limitation in the series of control rotors **3** was the lack of rotors with small R-groups (*B*-values < 7.4 kcal/mol) that would be close to the size of the R-groups in the chalcogen rotors **1** and **2**. Therefore, the acyclic oxygen rotors **2**(OCH_3) and **2**(OPh) were added to the steric control group (Figure 7, open triangles). We reasoned that these rotors were unlikely to form ChB interactions as they were acyclic rotors, which do not adopt the proper TS geometry. In addition, they contain the least polarizable and smallest chalcogen, oxygen, which was unlike to form ChB interactions without attached electron-withdrawing groups.[45,48] These hypotheses were confirmed as the rotational barriers for **2**(OCH_3) and **2**(OPh) fell on the steric trendline and extended the line to lower *B*-values. In addition, all of the ChB forming rotors had barriers that were lower than predicted by the steric trendline. The distance from the steric trendline, as calculated using equation 3, provided the TS stabilization energy by the ChB interaction.

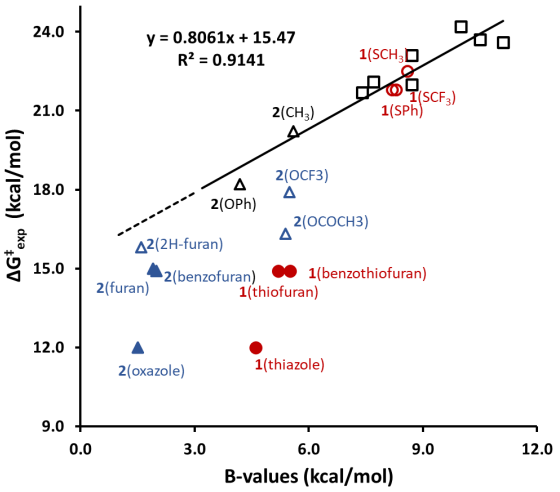

Fig. 7 Quantitative analysis of the measured rotational barriers ($\Delta G^{\ddagger}_{exp}$) versus the steric parameter (*B*-value) to isolate the repulsive steric and attractive ChB components of the rotational barriers. The steric trendline (black solid line) was generated from the control rotors **3** (open black squares) and acyclic oxygen rotors **2**(OCH_3) and **2**(OPh) (open black triangles). Deviations from the steric trendline on the y-axis provides a measure of the ChB interaction energy (E_{int}) for the cyclic sulfur rotors **1** (filled red circles), acylic sulfur rotors **1** (open red circles), cyclic oxygen rotors **2** (filled blue triangles) and acyclic oxygen rotors **2** with electron withdrawing groups (open blue triangles).

A key assumption in the above analysis was that variations in the rotational barriers were due only to variations in energy of the TS energies and that the ground state energies stay constant. This assumption was supported by energy decomposition analyses (ESI, Section 13) that showed that the calculated intramolecular TS interactions were strongly correlated with the experimentally measured interaction energies. More directly, the excellent correlation (R^2 = 0.914) of the $\Delta G^{\ddagger}_{exp}$ values for the steric control rotors **3** and non-interacting acyclic oxygen rotors **2**(OCH_3) and **2**(OPh) with the steric parameter *B*-value provided strong support for the ability to accurately model the barriers by examination of the TS interactions. This assumption was also supported by our previous studies that used a similar series of steric control rotors to successfully isolate the stabilizing TS interactions in the *N*-phenylsuccinimide rotors.[36–40]

Equation 3, which is derived from a combination of equations 1 and 2, was used to calculate the ChB interaction energies (E_{int}) for each of the chalcogen rotors (Table 1). The cyclic sulfur rotors **1**(thiofuran), **1**(benzothiofuran), **1**(thiazole), which had the best σ-hole alignment, had the strongest E_{int} values (-4.8 to -7.2 kcal/mol) which is consistent with the formation of strong stabilizing ChB interactions. In contrast, the acyclic sulfur rotors **1**(SCH_3), **1**(SPh), **1**(SCF_3) which had poor σ-hole alignment had very small E_{int} values of 0.1 to -0.4 kcal/mol. Thus, the analysis provided quantitative data to support our initial pairwise analyses.

The quantitative analyses also provided the means to answer the question of whether oxygen can form effective ChB interactions.[45,48] Oxygen is the least polarizable and most electronegative chalcogen and thus generally forms the weakest ChB interactions. However, oxygen is also the most abundant chalcogen and thus has considerable potential in ChB catalyst design. The E_{int} values (-1.1 to -4.7 kcal/mol) suggest that cyclic oxygen rotors **2**(2H-furan), **2**(furan), **2**(benzofuran), and **2**(oxazole) form weak to moderate ChB interactions. However, these E_{int} values have a higher degree of uncertainty than for the larger sulfur rotors. The cyclic oxygen rotors have very low *B*-values (1.5 to 2.1 kcal/mol) which extend below the range of the range of the experimentally measured *B*-values (4.2 to 11.5 kcal/mol) for the steric control rotors. Thus, their E_{int} values are based on extrapolations of the steric trendline which have higher degrees of uncertainty (See ESI, section 5). For example, the confidence interval for E_{int} is ±1.0 to ±1.5 kcal/mol in the low *B*-value range for the cyclic oxygen rotors (ESI, Figure S28 regression confidence line), which is similar in magnitude to the E_{int} values (-1.0 to -4.7 kcal/mol). So there was a high degree of uncertainty in establishing that the oxygen rotors were forming ChB interactions. For comparison, the confidence interval in the *B*-value range for the cyclic sulfur rotors is much smaller ±0.6 to ±0.8 kcal/mol especially comparison to the E_{int} values (-4.8 to -7.2 kcal/mol).

To better address the question of whether oxygen can form ChB interactions, oxygen rotors that former stronger ChB interactions, which would be outside of our uncertainty range, were examined. Electronegative and electron withdrawing groups are known to enhance the strength of ChB interactions by increasing the size of the σ-hole and the increasing the electrostatic positive charge of the chalcogen atom.[2,49] For example, the cyclic sulfur rotor which formed the strongest ChB interaction (E_{int} = -7.2 kcal/mol) was **1**(thiazole) which had an electronegative nitrogen in conjugation with the chalcogen sulfur atom. The oxygen rotors with enhanced ChB interactions included cyclic (**2**(oxazole)) and acyclic (**2**(OCF_3) and **2**($OCOCH_3$)) rotors.

The E_{int} values for cyclic oxygen rotors with electronegative groups showed an enhancement in the strength of the ChB, which was similar to the enhancement observed for the cyclic sulfur rotors. The conjugated electronegative nitrogen in **2**(oxazole) strengthened the intramolecular ChB interaction by 2.7 kcal/mol in comparison to **2**(furan) which lacked the heterocyclic nitrogen. A similar increase of 2.4 kcal/mol was observed for the analogous sulfur pair of **1**(thiazole) and **1**(thiofuran). More importantly, the strength of the oxygen ChB interaction was E_{int} = -4.7 kcal/mol, which was larger than the error of the analysis.

Interestingly, the electron withdrawing groups also enhanced the strength of the ChB interactions for the acyclic oxygen rotors. For example, the E_{int} of **2**(OCF_3) with a CF_3 electron withdrawing group was -2.2 kcal/mol lower than **2**(OCH_3). Likewise, the acetyl group lowered the $\Delta G^{\ddagger}_{exp}$ of **2**($OCOCH_3$) lower the barrier even further by -3.7 kcal/mol in comparison to **2**(OCH_3).

The analogous electron withdrawing group trends were not observed for in the acyclic sulfur rotors, which provided insight into the relative contributions of the orbital-orbital

(n→σ*) and electrostatic components. For the acyclic sulfur rotors, attaching a CF_3 group had only a small influence as the E_{int} of **1**(SCF_3) and **1**(SCH_3), which only differed by -0.3 kcal/mol. The origins of these differences in electron withdrawing groups trends for the sulfur and oxygen ChB interactions were investigated further in the next section.

In summary, the oxygen ChB interactions could be observed and measured by the molecular rotors. Oxygen formed weaker ChB interactions in comparison to sulfur as expected. In the absence of electron withdrawing groups, the oxygen ChB interactions were difficult to observe. However, with electron withdrawing groups the oxygen ChB interactions could be as strong as sulfur ChB interactions.

Analysis of orbital-orbital interactions

To assess the magnitude of the orbital component of the ChB interactions, Natural Bonding Orbital (NBO) analyses were performed on the TS structures. The second order perturbation interaction energies of the donor orbitals on the C=O oxygen and acceptor orbitals on the chalcogens were calculated for rotors **1** and **2** (Table 2), providing a comparison of the n→σ* interactions.[3,50] The NBO interaction energies were consistent with the experimental observations of the ChB interactions in the sulfur rotors **1**. A stabilizing NBO interaction (-5.8 to -6.9 kcal/mol) was observed for the cyclic sulfur rotors (**1**(thiofuran), **1**(benzothiofuran), **1**(thiazole)), which form ChB interactions. In contrast, the acyclic sulfur rotors, which do not form ChB interactions, had negligible NBO interaction energies (0.0 kcal/mol). The acyclic sulfur rotor **1**(SCH_3) was again an exception, as the NBO interaction energies depended on the TS geometry and the alignment of the sulfur σ*. The planar TS had an NBO interaction energy similar to the cyclic sulfur rotors; whereas, the perpendicular TS had an NBO interaction energy of zero.

In contrast, the NBO interaction energies for the oxygen rotors did not correlate with the observed E_{int} values. This is consistent with the oxygen ChB interaction having a small or negligible orbital component. The cyclic oxygen rotors had small NBO energies of 0.0 to -0.6 kcal/mol. Even **2**(oxazole) which showed moderate TS stabilization (E_{int} = -4.7 kcal/mol) had a very NBO energy of only -0.6 kcal/mol. Similarly, the acyclic oxygen rotor NBO energies were low regardless of the observed stabilization energies (E_{int}). For example, even the oxygen rotors with electron withdrawing groups (**2**(OCF_3) and **2**($OCOCH_3$)) and modest E_{int} values (-2.0 and -3.5) had negligible NBO energies (0.0 kcal/mol).

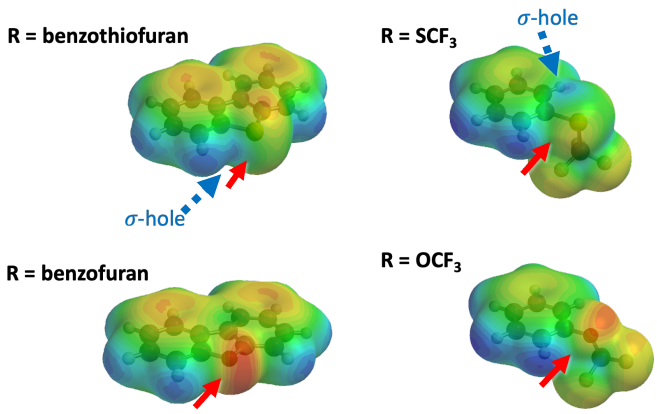

Fig. 8 Examples of the ESP surfaces generated for the *N*-phenyl units of rotors **1**(benzothiofuran), **1**(SCF_3), **2**(benzofuran), **2**(OCF_3). The calculations were performed without the norborene succinimide units to allow visualization of the interacting surface on the chalcogen atom. The position on the surface of the chalcogen used to estimate the ESP for each rotor is highlighted with a red arrow and corresponds to the approximate position of the C=O oxygen in the TS. The σ-hole of the sulfur R-groups are highlighted with a blue arrow. The oxygen R-groups did not have clearly defined σ-holes.

Electrostatic Potential Analysis

Next, we look for a simple parameter which could accurately predict the ChB interaction energies. This could be a useful tool for researchers designing new systems based on ChB interactions or optimize existing systems. The variability of the orbital component ruled out the use of NBO interaction energies. However, the ChB interactions of oxygen and sulfur rotors all appeared to have a strong electrostatic component. Therefore, we explored the ability of electrostatic potential (ESP) to predict the ChB interactions energies. Of the many electrostatic parameters, ESP has been shown to be effective in predicting non-covalent interaction trends as best highlighted by the work of Hunter.[51] ESP describes the electrostatic potential energy at points on a molecular surface and therefore provides a measure of interaction energies and geometry.

The ability of ESP to predict the ChB interaction energies was tested by correlating ESP with the experimentally measured E_{int} values. The ESP energies (Table 2) were calculated at the position on the surface of the chalcogen atom with the closest contact to the C=O oxygen in the TS structures. Examples are shown in Figure 8. The norbornene succinimide portions of the rotors were deleted because they blocked the region of the chalcogen unit that was involved in the ChB interaction.

An excellent correlation was observed between the chalcogen ESP and rotor E_{int} with an R^2 = 0.964 (Figure 9). The ESP trendline included both sulfur and oxygen rotors and also the cyclic and acyclic rotor, demonstrating the generality of the predictive parameter across different types of chalcogen bonding interactions. **Thus, ESP was an excellent predictor of the ability of ChB interactions to stabilize the bond rotation transition states.**

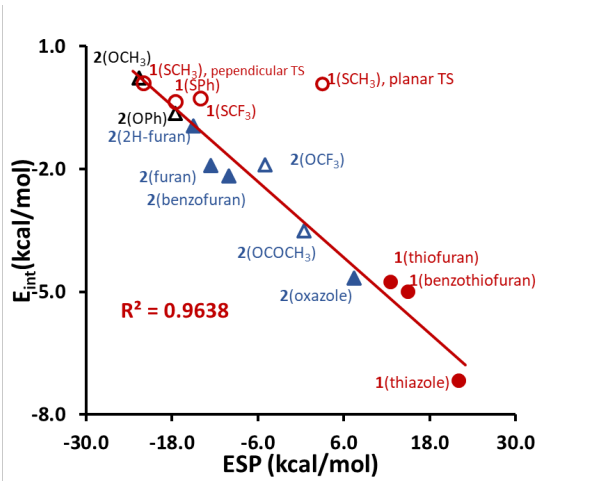

Fig. 9 Plot of electrostatic surface potentials (ESP, ωB97M-V/6-311+G*) versus the experimentally measured stabilizing TS interaction energies (E_{int}) for rotors **1** and **2**: acyclic oxygen rotors **2**(OCH_3) and **2**(OPh) (open black triangles), acylic sulfur rotors **1** (open red circles), cyclic oxygen rotors **2** (filled blue triangles), acyclic oxygen rotors **2** with electron withdrawing groups (open blue triangles) and cyclic sulfur rotors **1** (filled red circles).

The ability of ESP to simultaneously predict the ChB interaction energies of rotors that had strong and weak orbital components was surprising. For example, the cyclic sulfur rotors that have a significant orbital component such as **1**(benzothiofuran), **1**(thiofuran), and **1**(thiazole) fell on the same ESP trendline as the acyclic rotors that lack an orbital component such as **2**(OCF_3) and **2**($OCOCH_3$). In the case of the cyclic sulfur rotors, the position on the sulfur atom used to measure the ESP coincided with the σ-hole. An example is shown in Figure 8 (R = benzothiofuran) where the ESP position (red arrow) is the same as the σ-hole (blue arrow). However, the ESP position for the other types of rotors either did not correlate with the σ-hole (Figure 8, R =SCF_3) or the rotors laced a σ hole (Figure 8, R = benzofuran or OCF_3). **Thus, the effectiveness of ESP in predicting the ChB interaction energies regardless of the degree of orbital overlap suggest that the ESP values were either providing some measure of the orbital component or were correlated with the orbital interaction energies.**

The only outlier from the E_{int} vs ESP plot (Figure 9, open red circle) was, again, the planar TS of rotor **1**(SCH_3). An analysis of this deviation provided insight in the origins of the effectiveness of ESP as a predictive parameter. The ESP value for the planar TS of **1**(SCH_3) was +3.0 kcal/mol, which fell well off the trendline. By comparison, the ESP value for the perpendicular TS of **1**(SCH_3) was -22.0 kcal/mol which fell on the trendline. We hypothesized that the differences were due to ESP analysis only taking into account the TS stabilizing interactions. This is effective for the majority of the chalcogen R-groups, which adopt geometries that avoid strong repulsive interactions. The ESP of the planar TS is more positive than the perpendicular TS by 25.0 kcal/mol. This difference is consistent with the planar TS forming a chalcogen bonding interaction with the imide oxygen; whereas the perpendicular TS not having the proper orbital alignment to form an interaction. However, the planar TS of **1**(SCH_3) also forms form modest steric interactions (Figure 6a). Therefore, the ESP value does not directly correlate to the rotational barrier.

Contrasting components of the sulfur and oxygen ChB interactions

The above analyses revealed that sulfur and oxygen can form stabilizing ChB interactions, but the interactions differ in the balance of their orbital-orbital and electrostatic components, leading to different stability trends. The sulfur and oxygen ChB interactions both have strong electrostatic components. This is evident from the ability of the electrostatic parameter, ESP, to accurately predict the interaction energies, E_{int}, as shown in Figure 9. In contrast, the sulfur and oxygen ChB interactions have different orbital-orbital components as seen from the NBO secondary perturbation energies as shown in Table 2. The more polarizable sulfur had a well-defined σ^* and could form strong orbital-orbital interactions; whereas the less polarizable oxygen had a smaller σ^* and could not form strong orbital-orbital interactions. The differences in the orbital components are most clearly perceived in cyclic sulfur and oxygen rotors, which have their σ^*-orbitals aligned with the C=O oxygen lone pairs. The cyclic sulfur rotors **1** have significant NBO energies (-6.9 to -5.8 kcal/mol) as shown in Table 2. However, the cyclic oxygen rotors **2**, which have similar lone-pair to σ^*-orbital geometries, displace low or negligible NBO energies (-0.6 to 0 kcal/mol).

The differences in the orbital components are consistent with the differences in the polarizabilities of the sulfur and oxygen atoms. The more polarizable sulfur enables the formation of a significant σ^*-orbital. This can be seen by a well-formed σ-hole in the electrostatic surface maps of the sulfur groups (Figure 8, R = benzothiofuran). In contrast, the less polarizable oxygens lead to smaller σ^*-orbitals, and the corresponding oxygen σ-holes are not visible in the electrostatic surface maps (Figure 8, R = benzofuran).

These differences in the orbital-orbital and electrostatic component of the sulfur and oxygen ChB interactions also explain the different trends for the acyclic rotors. The significant orbital component of the sulfur ChB interaction leads to greater geometric constraints, requiring alignment of the donor lone pair with the chalcogen σ-hole. The importance of proper geometry is evident from the large differences in the interaction energies of the cyclic and acyclic sulfur rotors which have good and poor σ-hole alignments. In contrast, oxygen ChB interactions can adopt a wider variety of geometries. The electron-withdrawing effects of substituents are not focused on the σ-hole and are instead distributed more evenly across the oxygen atom surface.

Comparison of ChB with other non-covalent interactions

Our study of ChB interactions using the *N*-phenylsuccinimide rotors provided the opportunity to compare with non-covalent interactions. We have previously measured the TS stabilizing effects of $n\rightarrow\pi^*$(CO),[38] $n\rightarrow\pi$(Ph),[37] pnictogen bonds,[40] and hydrogen bonding interactions.[36] The interactions were measured

using the same rotor framework and formed interactions with the same succinimide C=O oxygens. What differs is the complementary acceptor group (S, O, N, C=O, Ph, HO) which has electrostatically positive π- or σ-hole region.

The relative TS stabilizing abilities of the interactions are shown in Figure 10. The C=O•••HO-Ph hydrogen bonds were the strongest. However, the remaining interactions, including the sulfur and oxygen chalcogen interactions, spanned a broad and overlapping range of interaction energies. The stability trends revealed some general trends. First, electronegative accepting groups and electron-withdrawing groups on the accepting groups enhanced the strength of the interactions. This is consistent with the interactions originating from donor-acceptor orbital-orbital and electrostatic interactions. For example, when comparing different types of pnictogen interactions, the electron-poor nitrogen of amides forms the strongest interactions, and the electron-rich nitrogen of amines form weaker interactions.[40] For the $n\rightarrow\pi^*$ interactions, the electron-poor carbonyl groups form stronger interactions than phenyl groups.[37,38] The same trends were observed for the ChB interactions. The electron withdrawing groups on the chalcogen atom such as CF_3 in rotors **2**(OCF_3) or conjugated electronegative nitrogen atoms in rotors **1**(thiazole) and **2**(oxazole) increase the strength of the interaction.

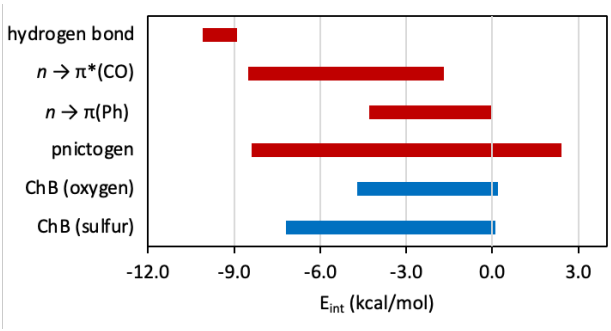

Fig. 10 Comparison of the TS stabilizing effects (E_{int}) measured in the *N*-phenylsuccinimide rotors of the oxygen and sulfur chalcogen bonding interactions in this study (blue bars) versus the previously measured $n\rightarrow\pi^*$(CO),[38] $n\rightarrow\pi$(Ph),[37] pnictogen,[40] and hydrogen bonding interactions[36] (red bars).

Conclusions

This study has demonstrated the potential of the chalcogen bonding interactions of oxygen and sulfur in facilitating kinetic processes and organocatalysis. Using *N*-phenylsuccinimide molecular rotors, the transition state stabilizing effects of chalcogen bonding interactions were measured and compared. Rotors with variations in the chalcogen atom orientation and electron-withdrawing groups were synthesized. The rotational barriers were measured using dynamic NMR. The formation of the intramolecular ChB interactions in the bond rotation transition states were verified from the experimental rotational barrier trends and computational modeling of the TS structures. Evidence for the ChB interactions were provided by the short atom-atom distances and correlation with proper alignment of the chalcogen σ-hole. The more polarizable sulfur rotors formed strong ChB interactions as expected. However, the oxygen rotors could also form ChB interactions if appropriate electronegative or electron withdrawing groups were present. Given the higher availability and better-established chemistry for incorporation of oxygen and sulfur functional into organic frameworks, these results suggest that new organic catalysts could be designed that utilize oxygen and sulfur ChB interactions.

The oxygen and sulfur ChB interactions had different geometric constraints due to the different strengths of their orbital-orbital components. The sulfur ChB interaction has a strong orbital component and thus is restricted to geometries where the lone pair donor orbital is aligned with the sigma-hole of the sulfur atom. The less polarizable oxygen atom does not form a significant sigma-hole in our systems and thus does not have a significant orbital component. However, this allows the oxygen ChB interaction to form in a wider array of geometries as the effects of electron withdrawing groups are more uniformly distributed on the chalcogen atom surface of the less polarizable oxygen. The ESP energy calculated at the interacting point on the surface of the chalcogen atom was an excellent predictive parameter for the strength and geometry of the interaction. Therefore, ESP can be used in designing and optimizing organocatalysts and reactions that involve ChB interactions.

Author contributions

Binzhou Lin and Hao Liu contributed equally.

Conflicts of interest

There are no conflicts to declare.

Acknowledgements

Funding for this work was provided by the National Science Foundation grants CHE 2003889 and 2304777.

Notes and references

1 C. B. Aakeroy, D. L. Bryce, G. R. Desiraju, A. Frontera, A. C. Legon, F. Nicotra, K. Rissanen, S. Scheiner, G. Terraneo, P. Metrangolo and G. Resnati, Definition of the chalcogen bond (IUPAC Recommendations 2019), *Pure Appl. Chem.*, 2019, **91**, 1889–1892.

2 P. Scilabra, G. Terraneo and G. Resnati, The Chalcogen Bond in Crystalline Solids: A World Parallel to Halogen Bond, *Acc. Chem. Res.*, 2019, **52**, 1313–1324.

3 L. Vogel, P. Wonner and S. M. Huber, Chalcogen Bonding: An Overview, *Angew. Chem. Int. Ed.*, 2019, **58**, 1880–1891.

4 R. Hein and P. D. Beer, Halogen bonding and chalcogen bonding mediated sensing, *Chem. Sci.*, 2022, **13**, 7098–7125.

5 P. C. Ho, P. Szydlowski, J. Sinclair, P. J. W. Elder, J. Kübel, C. Gendy, L. M. Lee, H. Jenkins, J. F. Britten, D. R. Morim and I. Vargas-Baca, Supramolecular macrocycles reversibly

assembled by Te…O chalcogen bonding, *Nat. Commun.*, 2016, **7**, 11299.

6 N. Biot and D. Bonifazi, Chalcogen-bond driven molecular recognition at work, *Coord. Chem. Rev.*, 2020, **413**, 213243.

7 R. Hein, P. D. Beer and J. J. Davis, Electrochemical Anion Sensing: Supramolecular Approaches, *Chem. Rev.*, 2020, **120**, 1888–1935.

8 B. R. Beno, K.-S. Yeung, M. D. Bartberger, L. D. Pennington and N. A. Meanwell, A Survey of the Role of Noncovalent Sulfur Interactions in Drug Design, *J. Med. Chem.*, 2015, **58**, 4383–4438.

9 H. Sugiyama, M. Yoshida, K. Mori, T. Kawamoto, S. Sogabe, T. Takagi, H. Oki, T. Tanaka, H. Kimura and Y. Ikeura, Synthesis and Structure Activity Relationship Studies of Benzothieno[3,2-b]furan Derivatives as a Novel Class of IKK.BETA. Inhibitors, *Chem. Pharm. Bull.*, 2007, **55**, 613–624.

10 B. V. McInerney, R. P. Gregson, M. J. Lacey, R. J. Akhurst, G. R. Lyons, S. H. Rhodes, D. R. J. Smith, L. M. Engelhardt and A. H. White, Biologically Active Metabolites from Xenorhabdus Spp., Part 1. Dithiolopyrrolone Derivatives with Antibiotic Activity, *J. Nat. Prod.*, 1991, **54**, 774–784.

11 A. Dhaka, O. Jeannin, I. Jeon, E. Aubert, E. Espinosa and M. Fourmigué, Activating Chalcogen Bonding (ChB) in Alkylseleno/Alkyltelluroacetylenes toward Chalcogen Bonding Directionality Control, *Angew. Chem. Int. Ed.*, 2020, **132**, 23789–23793.

12 M. Fourmigué and A. Dhaka, Chalcogen bonding in crystalline diselenides and selenocyanates: From molecules of pharmaceutical interest to conducting materials, *Coord. Chem. Rev.*, 2020, **403**, 213084.

13 M. Liu, X. Han, H. Chen, Q. Peng and H. Huang, A molecular descriptor of intramolecular noncovalent interaction for regulating optoelectronic properties of organic semiconductors, *Nat. Commun.*, 2023, **14**, 2500.

14 S. Benz, J. López-Andarias, J. Mareda, N. Sakai and S. Matile, Catalysis with Chalcogen Bonds, *Angew. Chem. Int. Ed.*, 2017, **129**, 830–833.

15 W. Wang, H. Zhu, S. Liu, Z. Zhao, L. Zhang, J. Hao and Y. Wang, Chalcogen–Chalcogen Bonding Catalysis Enables Assembly of Discrete Molecules, *J. Am. Chem. Soc.*, 2019, **141**, 9175–9179.

16 R. Weiss, E. Aubert, P. Pale and V. Mamane, Chalcogen-Bonding Catalysis with Telluronium Cations, *Angew. Chem. Int. Ed.*, 2021, **60**, 19281–19286.

17 W. Wang, H. Zhu, L. Feng, Q. Yu, J. Hao, R. Zhu and Y. Wang, Dual Chalcogen–Chalcogen Bonding Catalysis, *J. Am. Chem. Soc.*, 2020, **142**, 3117–3124.

18 S. Benz, J. Mareda, C. Besnard, N. Sakai and S. Matile, Catalysis with chalcogen bonds: neutral benzodiselenazole scaffolds with high-precision selenium donors of variable strength, *Chem. Sci.*, 2017, **8**, 8164–8169.

19 E. R. T. Robinson, C. Fallan, C. Simal, A. M. Z. Slawin and A. D. Smith, Anhydrides as α,β-unsaturated acyl ammonium precursors: isothiourea-promoted catalytic asymmetric annulation processes, *Chem. Sci.*, 2013, **4**, 2193.

20 V. B. Birman and X. Li, Benzotetramisole: A Remarkably Enantioselective Acyl Transfer Catalyst, *Org. Lett.*, 2006, **8**, 1351–1354.

21 V. B. Birman and L. Guo, Kinetic Resolution of Propargylic Alcohols Catalyzed by Benzotetramisole, *Org. Lett.*, 2006, **8**, 4859–4861.

22 V. B. Birman and X. Li, Homobenzotetramisole: An Effective Catalyst for Kinetic Resolution of Aryl-Cycloalkanols, *Org. Lett.*, 2008, **10**, 1115–1118.

23 X. He, X. Wang, Y.-L. S. Tse, Z. Ke and Y.-Y. Yeung, Applications of Selenonium Cations as Lewis Acids in Organocatalytic Reactions, *Angew. Chem. Int. Ed.*, 2018, **57**, 12869–12873.

24 P. Wonner, L. Vogel, F. Kniep and S. M. Huber, Catalytic Carbon-Chlorine Bond Activation by Selenium-Based Chalcogen Bond Donors, *Chem. Eur. J.*, 2017, **23**, 16972–16975.

25 P. Wonner, A. Dreger, L. Vogel, E. Engelage and S. M. Huber, Chalcogen Bonding Catalysis of a Nitro-Michael Reaction, *Angew. Chem. Int. Ed.*, 2019, **58**, 16923–16927.

26 L. Bao, X. Kong and Y. Wang, Noncovalent Chalcogen-Bonding Catalysis Using ppm-Level Catalyst Loading to Achieve Cyanosilylation of Ketones, *Asian J. Org. Chem.*, 2020, **9**, 757–760.

27 X. Kong, P. Zhou and Y. Wang, Chalcogen···π Bonding Catalysis, *Angew. Chem. Int. Ed.*, 2021, **60**, 9395–9400.

28 D. J. Pascoe, K. B. Ling and S. L. Cockroft, The Origin of Chalcogen-Bonding Interactions, *J. Am. Chem. Soc.*, 2017, **139**, 15160–15167.

29 G. E. Garrett, G. L. Gibson, R. N. Straus, D. S. Seferos and M. S. Taylor, Chalcogen Bonding in Solution: Interactions of Benzotelluradiazoles with Anionic and Uncharged Lewis Bases, *J. Am. Chem. Soc.*, 2015, **137**, 4126–4133.

30 F. De Vleeschouwer, M. Denayer, B. Pinter, P. Geerlings and F. De Proft, Characterization of chalcogen bonding interactions via an in-depth conceptual quantum chemical analysis, *J. Comput. Chem.*, 2018, **39**, 557–572.

31 Y. Nagao, T. Hirata, S. Goto, S. Sano, A. Kakehi, K. Iizuka and M. Shiro, Intramolecular Nonbonded S···O Interaction Recognized in (Acylimino)thiadiazoline Derivatives as Angiotensin II Receptor Antagonists and Related Compounds, *J. Am. Chem. Soc.*, 1998, **120**, 3104–3110.

32 C. M. Young, A. Elmi, D. J. Pascoe, R. K. Morris, C. McLaughlin, A. M. Woods, A. B. Frost, A. Houpliere, K. B. Ling, T. K. Smith, A. M. Z. Slawin, P. H. Willoughby, S. L. Cockroft and A. D. Smith, The Importance of 1,5-Oxygen···Chalcogen Interactions in Enantioselective Isochalcogenourea Catalysis, *Angew. Chem. Int. Ed.*, 2020, **59**, 3705–3710.

33 M. Iwaoka and S. Tomoda, Nature of the Intramolecular Se···N Nonbonded Interaction of 2-Selenobenzylamine Derivatives. An Experimental Evaluation by ^{1}H, ^{77}Se, and ^{15}N NMR Spectroscopy, *J. Am. Chem. Soc.*, 1996, **118**, 8077–8084.

34 S. Mehrparvar, C. Wölper and G. Haberhauer, Chalcogen-Bond-Induced Double Helix Based on Self-Assembly of a Small Planar Building Block, *Angew Chem Int Ed*, 2023, e202304202.

35 B. J. Eckstein, L. C. Brown, B. C. Noll, M. P. Moghadasnia, G. J. Balaich and C. M. McGuirk, A Porous Chalcogen-Bonded Organic Framework, *J. Am. Chem. Soc.*, 2021, **143**, 20207–20215.

36 E. C. Vik, P. Li, J. M. Maier, D. O. Madukwe, V. A. Rassolov, P. J. Pellechia, E. Masson and K. D. Shimizu, Large transition state stabilization from a weak hydrogen bond, *Chem. Sci.*, 2020, **11**, 7487–7494.

37 E. C. Vik, P. Li, D. O. Madukwe, I. Karki, G. S. Tibbetts and K. D. Shimizu, Analysis of the Orbital and Electrostatic Contributions to the Lone Pair–Aromatic Interaction Using Molecular Rotors, *Org. Lett.*, 2021, **23**, 8179–8182.

38 E. C. Vik, P. Li, P. J. Pellechia and K. D. Shimizu, Transition-State Stabilization by n→π* Interactions Measured Using Molecular Rotors, *J. Am. Chem. Soc.*, 2019, **141**, 16579–16583.

39 B. Lin, I. Karki, P. J. Pellechia and K. D. Shimizu, Electrostatically-gated molecular rotors, *Chem. Commun.*, 2022, **58**, 5869–5872.

40 B. Lin, H. Liu, I. Karki, E. C. Vik, M. D. Smith, P. J. Pellechia and K. D. Shimizu, Pnictogen Interactions with Nitrogen Acceptors, *Angew Chem Int Ed*, 2023, e202304960.

41 S. H. Alelaiwi and J. R. McKee, One-Pot Synthesis of Aminated Benzo-Fused Heterocycles and N-Substituted Dibenzothiophenes via Copper-Catalyzed Ullmann Type Reaction, *ACS Omega*, 2021, **6**, 6009–6016.

42 A. M. Schoevaars, W. Kruizinga, R. W. J. Zijlstra, N. Veldman, A. L. Spek and B. L. Feringa, Toward a Switchable Molecular Rotor. Unexpected Dynamic Behavior of Functionalized Overcrowded Alkenes, *J. Org. Chem.*, 1997, **62**, 4943–4948.

43 A. Ciogli, S. Vivek Kumar, M. Mancinelli, A. Mazzanti, S. Perumal, C. Severi and C. Villani, Atropisomerism in 3-arylthiazolidine-2-thiones. A combined dynamic NMR and dynamic HPLC study, *Org. Biomol. Chem.*, 2016, **14**, 11137–11147.

44 L. Lunazzi, M. Mancinelli, A. Mazzanti, S. Lepri, R. Ruzziconi and M. Schlosser, Rotational barriers of biphenyls having heavy heteroatoms as ortho-substituents: experimental and theoretical determination of steric effects, *Org. Biomol. Chem.*, 2012, **10**, 1847.

45 T. Fellowes, B. L. Harris and J. M. White, Experimental evidence of chalcogen bonding at oxygen, *Chem. Commun.*, 2020, **56**, 3313–3316.

46 P. Politzer, J. S. Murray, T. Clark and G. Resnati, The σ-hole revisited, *Phys. Chem. Chem. Phys.*, 2017, **19**, 32166–32178.

47 R. E. Rosenfield, R. Parthasarathy and J. D. Dunitz, Directional preferences of nonbonded atomic contacts with divalent sulfur. 1. Electrophiles and nucleophiles, *J. Am. Chem. Soc.*, 1977, **99**, 4860–4862.

48 P. R. Varadwaj, A. Varadwaj, H. M. Marques and P. J. MacDougall, The chalcogen bond: can it be formed by oxygen?, *Phys. Chem. Chem. Phys.*, 2019, **21**, 19969–19986.

49 A. Docker, C. H. Guthrie, H. Kuhn and P. D. Beer, Modulating Chalcogen Bonding and Halogen Bonding Sigma-Hole Donor Atom Potency and Selectivity for Halide Anion Recognition, *Angew. Chem. Int. Ed.*, 2021, **60**, 21973–21978.

50 J. Y. C. Lim and P. D. Beer, Sigma-Hole Interactions in Anion Recognition, *Chem*, 2018, **4**, 731–783.

51 C. A. Hunter, Quantifying Intermolecular Interactions: Guidelines for the Molecular Recognition Toolbox, *Angew. Chem. Int. Ed.*, 2004, **43**, 5310–5324.